Spin-dynamics study of the classical ferromagnetic XY chain

R. W. Gerling and D. P. Landau
Center for Simulational Physics, University of Georgia, Athens, Georgia 30602
(Received 24 July 1989)

The time-dependent behavior of the classical, ferromagnetic xy chain in a symmetry-breaking magnetic field was studied using a very fast, vectorized spin-dynamics method. The equations of motion were integrated using starting configurations determined by Monte Carlo simulations. By calculating spin-spin correlation functions and taking space-time Fourier transforms, we determined $S(q,\omega)$ for a wide range of fields and temperatures. We identify and measure the characteristics of single spin-wave peaks and two spin-wave sum peaks, as well as central peaks due to both soliton and two spin-wave difference processes. These results are discussed in light of existing theory and experiments.

I. INTRODUCTION

The interest in the study of classical magnetic chains has been great over the past few years. The reason for this is twofold: first, there exist beautiful experimental results[1-7] for quasi-one-dimensional systems, and, second, there are detailed theoretical predictions[8-10] obtained by mapping an easy-plane spin chain onto the sine-Gordon model. Extensive investigations using a variety of methods followed, but the situation was complicated by differences between physical systems and theoretical models, quantum corrections, and finite-size effects.[11] From the experimental side the main difficulty is the measuring of the neutron scattering law $S(q,\omega)$: with the q vector parallel to one of the three axes only the sum of the polarizations of the two other axes can be measured. The decomposition into single polarizations introduces huge errors. The main interest of these studies was focused on the soliton-induced central peak. Because the background in these experiments is largest for $\omega=0$, $q=0$ extra errors are added. In a computer simulation these problems do not exist: the simulation is an ideal perfect experiment with all parameters controlled, and all polarizations can be measured directly. We have been using extensive computer simulations[12-18] to study the classical ferromagnetic XY chain in a symmetry-breaking magnetic field, because it is the model with the smallest number of adjustable parameters. By comparing the results of our simulation to the theoretical predictions, all the problems just mentioned are bypassed, and we can directly test the validity of the sine-Gordon theory for classical systems. The Hamiltonian of the XY chain is given by

$$\mathcal{H}_{xy}=-J\sum_{i=1}^{N}(S_i^xS_{i+1}^x+S_i^yS_{i+1}^y)-h\sum_{i=1}^{N}S_i^x\ , \qquad (1)$$

where the $\mathbf{S}_i$ are three-dimensional classical vectors of unit length, J is the exchange-coupling constant, and $h=g\mu_BH$ is an external magnetic field in the x direction. The exchange anisotropy makes it energetically favorable for the spins to lie in the xy plane, and the magnetic field tends to align the spins parallel to the positive x axis. We have previously reported results of simulations using less sophisticated techniques[17,18] which showed clear spin-wave peaks in $S(q,\omega)$ but had insufficient accuracy to resolve soliton central peaks even though solitons could be seen in microscopic spin configurations. In Sec. II of this paper we present details of the simulational method used, and include a discussion of the quality of the method. A short overview of the theoretical predictions is presented in Sec. III. Finally we present the results of our simulations in Sec. IV, and conclude in Sec. V.

II. METHOD

A standard importance sampling Monte Carlo[19] technique was used to generate equilibrium spin configurations for particular values of T and h with a chain length of typically $N=20\,000$ sites and a periodic boundary. Spin updates were performed using a two-sublattice decomposition and a vectorized algorithm on a CDC Cyber 205. The first 3000 Monte Carlo steps (MCS)/site were always discarded to insure that the system had reached equilibrium and then ten spin configurations, each separated by 200 MCS/site, were chosen as starting configurations for the spin-dynamics calculation. (We have tested that the correlation times are sufficiently short and that the separation by 200 MCS/site insures that the configurations were uncorrelated for our choice of parameters.) Averaging the results over many starting configurations is essentially equivalent to performing an ensemble average at the temperature for which the Monte Carlo run was carried out.

The equation of motion for each spin in the xy model is[17]

$$\dot{\mathbf{S}}_i=\mathbf{S}_i\times[J(S_{i+1}^x+S_{i-1}^x)\mathbf{e}_x+J(S_{i+1}^y+S_{i-1}^y)\mathbf{e}_y+h\mathbf{e}_x]\ , \qquad (2)$$

where $\mathbf{e}_x$, $\mathbf{e}_y$, and $\mathbf{e}_z$ are unit vectors in the x, y, and z directions. The coupled nonlinear equations of motion were integrated using a newly vectorized high-speed fourth-order predictor-corrector method[20] and a time integration interval $\Delta=0.01/J$. Since the algorithm is not

self-starting, the first few time steps were integrated using a fourth-order Runge-Kutta method. Each start configuration was integrated out to time $t_{\max}=100/J$.

For each time integration we calculated the time- and space-dependent spin-spin correlation functions

$$\langle S_i^k(0)S_{i+r}^k(t)\rangle=\frac{1}{N}\sum_{i=1}^{N}S_i^k(0)S_{i+r}^k(t)-\langle S_i^k(0)\rangle^2 , \quad (3)$$

where r is the distance measured in lattice spacings and $k=x,y,z$ denotes the polarization. The squared magnetization $\langle S_i^k(0)\rangle^2$ is subtracted to avoid problems in performing the Fourier transformation. The correlation functions were averaged over the ten starting configurations and then used as input for the last step of the program, which performed a double Fourier transform to yield the scattering law $S_k(q,\omega)$. To reduce cutoff effects we introduced a Gaussian spatial and temporal resolution function. We first performed the space Fourier transform

$$\langle S(-q,0)S(q,t)\rangle_k=\tfrac{1}{2}\langle S_i^k(0)S_i^k(t)\rangle + \sum_{r=1}^{r_{\max}}\cos(qr)\langle S_i^k(0)S_{i+r}^k(t)\rangle \times\exp[-\tfrac{1}{2}(r\delta r)^2] , \quad (4)$$

where the sum over r runs typically over $r_{\max}=200$ neighbors. The spatial cutoff parameter δr was chosen carefully to eliminate wiggles due to taking the Fourier transform of a function with a step (i.e., at $r_{\max}$) and also to avoid excessive broadening of any structure. We found $\delta r=0.015$ to be a good compromise. After the space Fourier transform the time Fourier transform was determined by the integral

$$S_k(q,\omega)=\left[\frac{2}{\pi}\right]^{1/2}\int_0^{t_{\max}}\cos(\omega t)\langle S(-q,0)S(q,t)\rangle \times\exp[-\tfrac{1}{2}(t\delta t)^2]dt \quad (5)$$

which was discretized for the actual numerical calculation. The temporal cutoff parameter δt was chosen independently and we found $\delta t=0.02J$ to be a good value. We have extensively tested the algorithm to insure that it works properly. A simple check such as monitoring the constants of motion is a necessary, but not sufficient, test. Results for different time integration intervals Δ were compared to insure that the correlations did not depend significantly on Δ. As a further test we integrated the equations of motion out to $t_{\max}=100/J$ with $\Delta=0.10/J$; we then negated the time increment to $\Delta=-0.01/J$ and integrated back to $t_{\text{start}}=0$ using the same number of integration steps. If the algorithm is working correctly, the starting configuration should be reproduced. The correlation of the starting configuration with the *reproduced* starting configuration should be one and any deviation from one is a sensitive measure of the quality. We find the deviation from one to be in the range from 3.8×10^{-2} to 2.7×10^{-4}, and the length of an individual spin changed less than 10^{-7}. The limiting feature of the spin-dynamics simulations was not the time integration routine but rather the number of start configurations which were used. Two different runs, each of which included averages of ten configurations, showed small, but distinct, differences. More initial states must be used to provide a better description of the equilibrium distribution of states before further improvement of the time integration method can be used to advantage.

In order to measure the intrinsic parameters of the line shapes in the simulational results for $S(q,\omega)$ we had to deconvolute the resolution functions. We therefore fitted our data with a Gaussian or Lorentzian line shape convoluted with our Fourier transformed resolution functions. This procedure is well established in the analysis of experimental neutron scattering data, where the resolution function of the spectrometer has to be taken into account.[21] We fitted the expression

$$S(q,\omega)=\frac{1}{2\pi\delta t\,\delta r}\int_{-\infty}^{\infty}\int_{-\infty}^{\infty}\exp\left[-\frac{(q'-q)^2}{2\delta r^2}\right] \times\exp\left[-\frac{(\omega'-\omega)^2}{2\delta t^2}\right] \times p(q',\omega')dq'd\omega' , \quad (6)$$

where

$$p(q',\omega')=\frac{I_L}{\pi^2}\frac{\kappa}{(q'^2+\kappa^2)}\frac{\Gamma_\omega}{(\omega'-\omega_{q'})^2+\Gamma_\omega^2} \quad (7a)$$

in the case of a Lorentzian line shape and

$$p(q',\omega')=\frac{\sqrt{\ln 2}I_G}{\sqrt{\pi}\sigma_\omega}\exp\left[-\ln 2\frac{\omega'^2}{\sigma_\omega^2}\right] \quad (7b)$$

in case of a Gaussian line shape. Here Γ_ω and σ_ω are the half-width of the peaks and I_L and I_G are the intensities of the peaks; κ is the inverse correlation length of the spin-spin correlation function. In (7a) we used a linearized version of the dispersion relation

$$\omega_q=\omega_{q_0}+\omega_{\text{slope}}(q-q_0) .$$

In the case of $S_y(q,\omega)$ we fitted the sum of a Lorentzian and a Gaussian line shape (the sum was taken after the convolution) to the data points.

III. THEORY

Excitations in magnetic chains in a field have been studied by Mikeska[8] who mapped the anisotropic Heisenberg chain onto the classical sine-Gordon model in an attempt to understand the magnetic excitations. The classical sine-Gordon system is described by the Hamiltonian

$$\mathcal{H}_{\text{sG}}=\int_{-L/2}^{+L/2}\frac{dx}{a}\left[\tfrac{1}{2}(\phi_t)^2+\frac{c^2}{2}(\phi_x)^2 +(mc)^2\{1-\cos[\phi(x)]\}\right] , \quad (8)$$

where m is the mass and c the characteristic velocity of

the solitons. The integration is along the chain of length L and a defines the length scale (lattice constant) and the subscripts denote partial derivatives. This model was studied extensively[22–24] including additional correction terms. The simplest excitations in this system are the following.

(i) Solitons (or antisolitons): localized excitations with a rest energy $8mc^2$ and a width of $2m^{-1}$, moving relativistically with a velocity $v < c$.

(ii) Spin waves: plane-wave solutions with a wave vector q and a dispersion $\omega(q)$.

The existence of spin solitons was demonstrated by directly looking at plots of the phase of the spins in the xy plane.[12,14] In the lowest order these excitations do not interact and it is possible to calculate the neutron scattering law $S(q,\omega)$ in this approximation. Allroth and Mikeska[9] also calculated higher-order contributions especially the spin-wave–spin-wave interaction. Summarizing the different results one finds the following contributions to the scattering law.

(1) $S_x(q,\omega)$: A central non-interacting-soliton peak $S_x^{\rm sol}(q,\omega)$ and the sum and difference two-spin-wave processes $S_x^{\rm sum}(q,\omega)$ and $S_x^{\rm diff}(q,\omega)$, respectively.

(2) $S_y(q,\omega)$: A central non-interacting-soliton peak $S_y^{\rm sol}(q,\omega)$ and a single spin-wave peak $S_y^{SW}(q,\omega)$.

(3) $S_z(q,\omega)$: The sine-Gordon theory restricts spins to the xy plane, but on general grounds we expect to see fluctuations out of plane which at least give rise to a single spin-wave peak $S_z^{\rm SW}(q,\omega)$.

Allroth and Mikeska[9] discussed the different line shapes within the sine-Gordon approximation of the xy model. The single spin-wave peak is a simple δ function

$$S_y^{\rm SW}(q,\omega)=\frac{k_BT}{4\pi(m^2+q^2)}\delta(\omega-\omega_q)\ , \tag{9}$$

where m is the rest mass of the solitons. Due to spin-wave interactions, the δ function becomes Lorentzian, i.e.,

$$\delta(\omega-\omega_q)\rightarrow\frac{1}{\pi}\frac{\Gamma}{(\omega-\omega_q)^2+\Gamma^2}\ .$$

The central soliton peak has a Gaussian line shape

$$S_\alpha^{\rm sol}(q,\omega)=\left[1-\frac{k_BT}{2m}\left[1-\frac{m^2+q^2}{12m^2}\right]\right]\frac{32}{cq\pi m^2}\left[\frac{m}{\pi k_BT}\right]^{1/2} n\exp\left[-\frac{4m\omega^2}{k_BTc^2q^2}\right]f_\alpha(q)\ , \tag{10}$$

where the function $f_\alpha(q)$ is given by

$$f_x(q)=\left[\frac{\pi q}{2m\sinh(\pi q/2m)}\right]^2\ , \tag{11a}$$

$$f_y(q)=\left[\frac{\pi q}{2m\cosh(\pi q/2m)}\right]^2\ , \tag{11b}$$

and n is the density of solitons, which is given by

$$n=4m\left[\frac{m}{\pi k_BT}\right]^{1/2}\exp\left[\frac{-8m}{k_BT}\right]\ . \tag{12}$$

These two line shapes are simple enough so that one can readily fit the numerical data with these predictions. We did this just using the predicted form for the line shape but not constraining the parameters. The two-spin-wave processes contribute much more complicated line shapes to the scattering law. The sum process shows a square-root singularity when $\omega=2\omega_{q/2}$ is approached from above:

$$S_x^{\rm sum}(q,\omega)=\frac{(ck_BT)^2}{8\pi^2}\frac{1}{\omega_{Q-q/2}\omega_{Q+q/2}}\left[\frac{\Theta(|\omega|-2\omega_{q/2})}{\omega_{Q-q/2}(Q+q/2)+\omega_{Q+q/2}(Q-q/2)}\right]\ , \tag{13a}$$

and the difference process produces an almost steplike central peak with the step at $\omega=cq$:

$$S_x^{\rm diff}(q,\omega)=\frac{(ck_BT)^2}{8\pi^2}\frac{1}{\omega_{Q-q/2}\omega_{Q+q/2}}\left[\frac{\Theta(cq-|\omega|)}{\omega_{Q-q/2}(Q+q/2)-\omega_{Q+q/2}(Q-q/2)}\right]\ , \tag{13b}$$

where

$$Q=\frac{|\omega|}{2c}\left[1+\frac{4m^2c^2}{c^2q^2-\omega^2}\right]^{1/2} \tag{14}$$

and

$$\Theta(x)=\begin{cases}0 & \text{for } x<0\ ,\\ 1 & \text{for } x\geq 0\ .\end{cases} \tag{15}$$

The expressions for these two strange line shapes are valid only within the approximation used by Allroth and Mikeska so it is not possible to improve the agreement

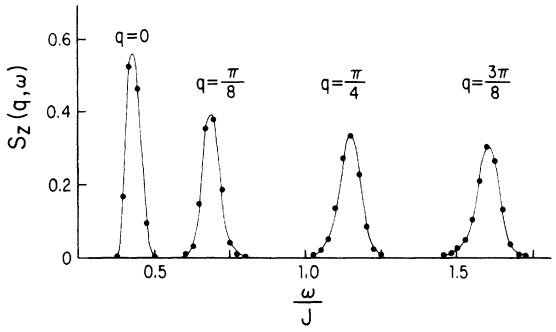

FIG. 1. $S_z(q,\omega)$ as a function of ω for different values of the wave vector. The temperature $k_BT=0.1J$ and the magnetic field $h=0.1J$. The lines are best fits of Lorentzian line shapes (convoluted with the Gaussian resolution function) to the data.

between the prediction and the numerical results by simply using better dispersion relations ω_q (e.g., the relation resulting from the simulation) in Eq. (13).

The different contributions to the central peak in $S(q,\omega)$ show characteristically different T and q dependences of the integrated intensity I_{CP} and the half-width at half maximum (HWHM) Γ_{CP}. The corresponding formulas can be derived from Eqs. (9) and (10). For the HWHM we get

$$\Gamma_{CP}^{sol}=\frac{cq}{2}\left[\frac{\ln 2}{m}\right]^{1/2}\sqrt{k_BT}\ , \tag{16a}$$

$$\Gamma_{CP}^{diff}\approx cq\ . \tag{16b}$$

The HWHM of the single spin-wave peak is given explicitly in Ref. 9:

$$\Gamma^{SW}=\frac{4n}{m}\omega_q\left[\frac{mc}{\omega_q}\right]^3\left[\frac{1}{2\sqrt{\beta m\pi}}+\frac{cq}{\omega_q}\right]\ . \tag{16c}$$

For the integrated intensities we obtain

$$I_{CP}^{sol}=\frac{32}{(\pi^3k_BTm)^{1/2}}\exp\left[\frac{-8m}{k_BT}\right]f_k(q)\times\left[1-\frac{k_BT}{2m}\left[1-\frac{m^2+q^2}{12m^2}\right]\right]\ , \tag{17a}$$

$$I_{CP}^{diff}=2I^{sum}=\frac{1}{32\pi m^3}\frac{(k_BT)^2}{2+(q/2m)^2}\ , \tag{17b}$$

$$I^{SW}=\frac{1}{4\pi}\frac{k_BT}{m^2+q^2}\left[1-\frac{4nm}{m^2+q^2}\left[1+\frac{4q^2}{3m^2}\right]\right]\ . \tag{17c}$$

Allroth and Mikeska do not derive an explicit line shape of the single spin-wave peak but merely give values for Γ^{SW} and I^{SW}.

The connection between the sine-Gordon system with the parameters c and m and the xy spin-system with the parameters J and h is made by the two relations

$$c=\sqrt{2}J\ ,\qquad m=\sqrt{h/J}\ , \tag{18}$$

where we already used the fact that $|\mathbf{S}|=1$. The anisotropy of the XY model is larger than the anisotropy of the easy-plane Heisenberg model thus yielding smaller out-of-plane fluctuations. Therefore, the agreement between the sine-Gordon approximation and the XY model should be better than between the sine-Gordon approximation and the one-dimensional easy-plane Heisenberg system, which is used to describe $CsNiF_3$. (The XY model corresponds roughly to an easy-plane Heisenberg system with anisotropy parameter $A=J$, whereas in $CsNiF_3$ $A\approx 0.2J$.)

IV. RESULTS

The neutron scattering law with polarization along the chain axis $S_z(q,\omega)$ is expected to show single spin-wave excitations, and indeed the results of the simulation show a clear, narrow single peak for each q value. In Fig. 1 we have plotted the peaks for four different q vectors parallel to the chain axis for $k_BT=0.1J$. All data points are averages over two simulations (each of which themselves represented averages over ten chains), and the scatter between different runs provides estimates for the error of the data points. The solid lines in Fig. 1 are fits to the data using a Lorentzian line shape convoluted with the Gaussian "instrumental" resolution function.[21] From the positions of the maxima the dispersion relation was accurately determined and we could also follow the softening of the entire dispersion relation with increasing temperature. The peak for $q=0$ has essentially zero intrinsic width and the entire observed width is due to the

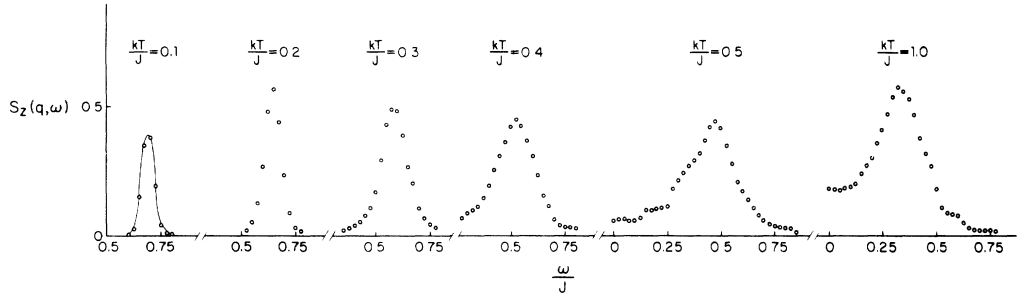

FIG. 2. $S_z(q,\omega)$ as a function of ω for different temperatures k_BT as indicated. The wave vector $qa=\pi/8$ and the magnetic field $h=0.1J$. The curve is the fitted intensity obtained by convoluting a Lorentzian and the Gaussian resolution function.

instrumental resolution function. The peaks broaden with increasing value of q. The uncertainty in the data points is of the order of the symbol size. At higher temperatures the peaks in $S_z(q,\omega)$ broaden noticeably and become slightly asymmetric for intermediate q values. Calculations by Reiter[25] for the easy-plane Heisenberg system indicate that this asymmetry might have its origin in a singularity in the three spin-wave density of states.

Figure 2 shows $S_z(q,\omega)$ as a function of ω for $qa=\pi/8$, $h=0.1J$ and different temperatures as indicated. The solid line for $k_BT=0.1J$ shows a best fit with an intrinsic line shape which is Lorentzian. With increasing temperature the peak position shifts to lower ω and the peak broadens. At the same time the peak becomes asymmetric and it is impossible to make any descent fit with a Lorentzian line shape. This peak remains quite visible even at the highest temperature studied.

The scattering function with the polarization perpendicular to both the chain axis and the magnetic field $S_y(q,\omega)$ is expected[9] to show a purely soliton-induced central peak in addition to a single-spin-wave peak. In Fig. 3 we show a typical result for $S_y(q,\omega)$ for $k_BT=0.4J$ where the soliton contribution is substantial. The spin-wave peak is at the frequency $\omega=0.525J$. Unlike the spin-wave peak, which is quite smooth, the central peak still possesses remnants of the oscillations produced by the finite time cutoff of the time integration. (Without the resolution function these oscillations are pronounced.) We fitted the data with a Gaussian line shape for the central peak and a Lorentzian for the one-spin-wave peak (dashed lines in Fig. 3) both of which are resolution broadened. The sum of the two contributions (solid line in Fig. 3) reproduces the data very well. In Fig. 4 we show $S_y(q,\omega)$ for $qa=\pi/8$, $h=0.1J$ and

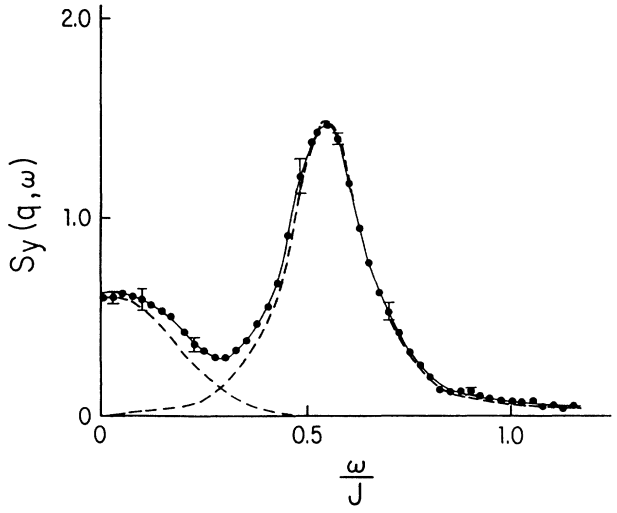

FIG. 3. $S_y(q,\omega)$ as a function of ω. The value of the wave vector $qa=\pi/8$. The temperature $k_BT=0.4J$ and the magnetic field $h=0.1J$. The dashed lines are best fits of a resolution broadened Gaussian central peak and a resolution broadened Lorentzian line shape to the data. The solid lines is the sum of the two contributions. Error bars are shown at some representative points.

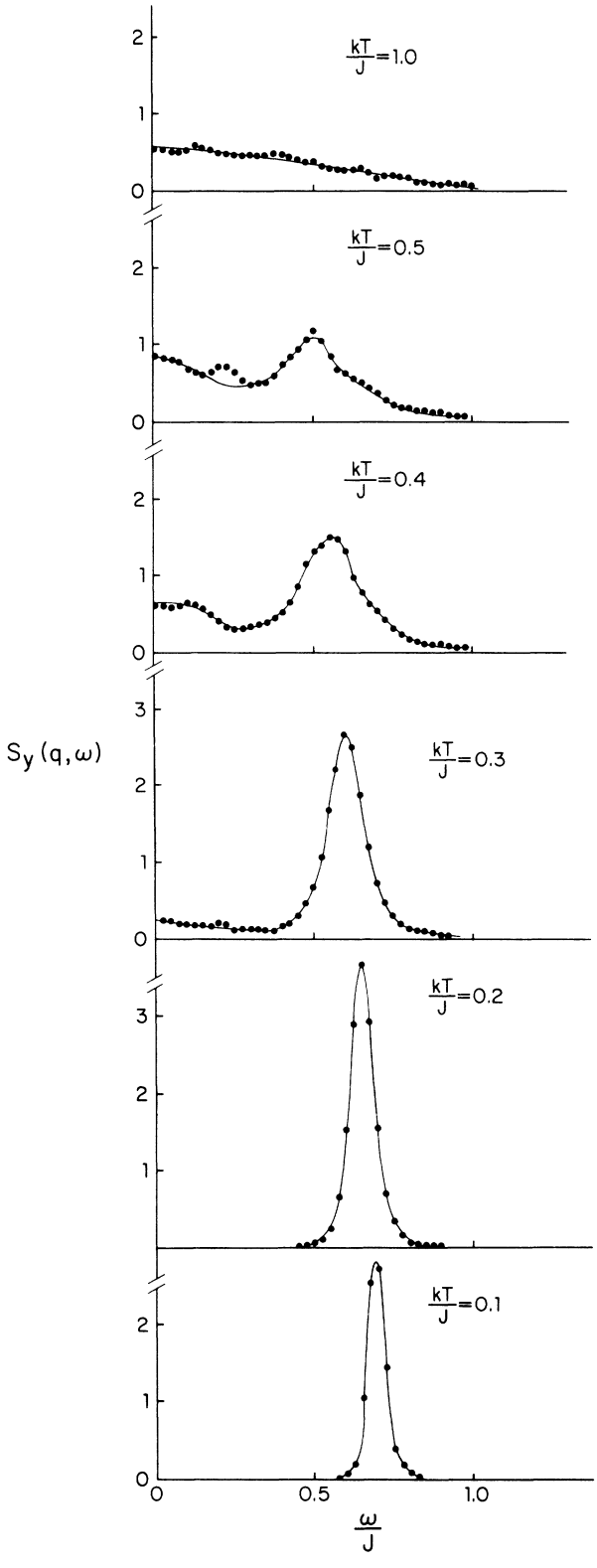

FIG. 4. $S_y(q,\omega)$ as a function of ω for different temperatures k_BT as indicated. The wave vector $qa=\pi/8$ and the magnetic field $h=0.1J$. The solid curves are fitted intensities representing the sum of resolution broadened Gaussian central peaks and Lorentzian spin-wave peaks.

different temperatures as indicated. At $k_BT=0.1J$ the soliton contribution is not visible at all. Only a single-spin-wave peak at $\omega=0.692J$ is present and it can be fitted very well by a resolution broadened Lorentzian. Due to an exponentially increasing soliton density at higher temperature, a very pronounced central peak quickly appears in addition to the spin-wave peak. At $k_BT=0.4J$ the linewidth of the spin-wave peak is just over double that observed for $k_BT=0.1J$. The solid line is the result of a best fit and is the sum of a Lorentzian and a Gaussian central peak, both of which are resolution broadened. At high temperatures, e.g., $k_BT=1.0J$ shown in Fig. 4, the behavior is purely diffusive with no spin-wave peaks visible in contrast to the behavior of $S_z(q,\omega)$ (cf. Fig. 2). In Fig. 5, $S_y(q,\omega)$ is shown for different magnetic fields at a temperature $k_BT=0.4J$. The soliton peak disappears rapidly with increasing magnetic field until, at $h=0.3J$, practically no central peak is left. The spin-wave peak is also shifted to larger values of ω with increasing field. The solid lines are a best fit. Finally, in Fig. 6, $S_y(q,\omega)$ is shown for different values of the wave vector qa. The temperature is $k_BT=0.4J$ and the magnetic field is $h=0.1J$. Again the central soliton peak decays with increasing wave vector. The dashed lines show the separated contributions from the two peaks.

In Fig. 7 we show $S_x(q,\omega)$ for $qa=\pi/8$, $h=0.1J$ and different temperatures as indicated. The neutron scattering function with polarization along the field axis $S_x(q,\omega)$ is predicted by Allroth and Mikeska[9] to exhibit a combination of soliton and two-spin-wave contributions. For $k_BT\leq 0.3J$ the soliton contribution is negligible, because the soliton density falls off exponentially with temperature, and one sees only the sum and difference two-spin-wave processes. Allroth and Mikeska evaluated the two-spin-wave process in the sine-Gordon model and found two contributions due to the spin-wave interactions: An almost step-function-like central peak for the difference process and a square-root singularity as $\omega=2\omega_{q/2}$ is approached from above, for the sum process. For the two lowest temperatures this behavior can indeed be observed, but starting with $k_BT=0.3J$ the soliton central peak begins to dominate. Because of the complicated line

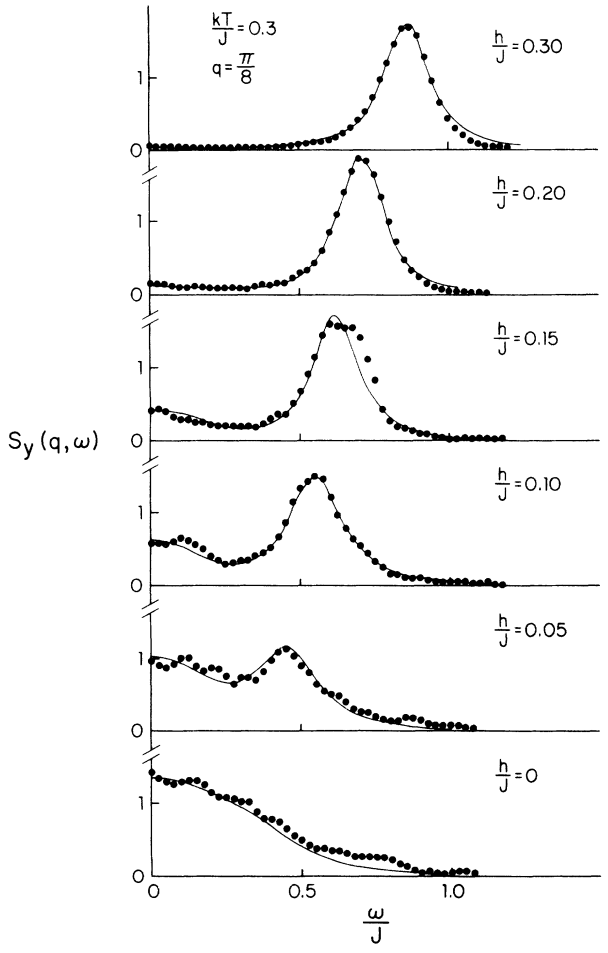

FIG. 5. $S_y(q,\omega)$ as a function of ω for different magnetic fields h as indicated. The temperature $k_BT=0.4J$ and the wave vector $qa=\pi/8$. The solid curves are fitted intensities representing the sum of resolution broadened Gaussian central peaks and Lorentzian spin-wave peaks.

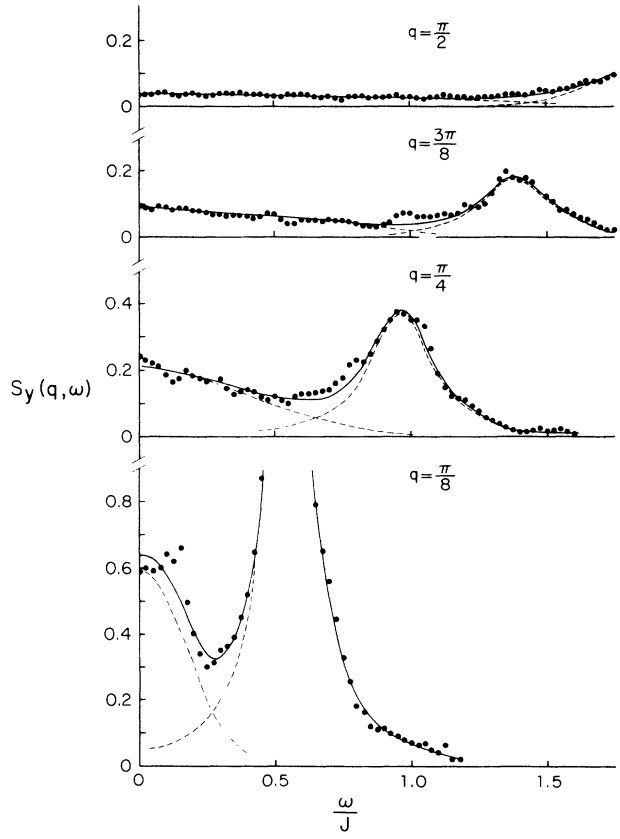

FIG. 6. $S_y(q,\omega)$ as a function of ω for different q as indicated. The temperature $k_BT=0.4J$ and the magnetic field $h=0.1J$. The solid curves are fitted intensities representing the sum of resolution broadened Gaussian central peaks and Lorentzian spin-wave peaks. The dashed curves indicated the single contributions.

shape of the two-spin-wave processes a fit of the data to a simple form is not possible. In Fig. 8 we show $S_x(q,\omega)$ for different magnetic fields. The temperature $k_BT=0.4J$ and $qa=\pi/8$. The arrows indicate the predicted positions of the expected two-spin-wave sum process, where the value $2\omega_{q/2}$ was determined from the dispersion relation. The dispersion for $k_BT=0.2J$ and $h=0.1J$ is shown in Fig. 9. For comparison we show the result from a harmonic approximation of the system (solid curve) and the dispersion of spin waves in the sine-Gordon system (dashed curve). The spin-dynamics data show a clear reduction of the energy to lower values over the entire Brillouin zone.

In Fig. 10 we make a direct comparison between our simulation results and the prediction from Allroth and Mikeska.[9] To compare our results with the analytical predictions, we multiplied their formulas with $(2\pi^3)^{1/2}$ to take into account different conventions for the Fourier transforms in our Eqs. (4) and (5) and in Eq. (1.13) in Ref. 9. The difference between two theoretical curves is the use of different dispersion relations: for the solid curve we used the harmonic approximation result, and for the dashed curve we used the sine-Gordon result. Both curves represented intrinsic shapes convoluted with the resolution function. The qualitative agreement between this prediction and our results is excellent. The predicted characteristic frequency $2\omega_{q/2}=2\times0.49J$ (the value for $\omega_{q/2}$ was determined from the dispersion relation which

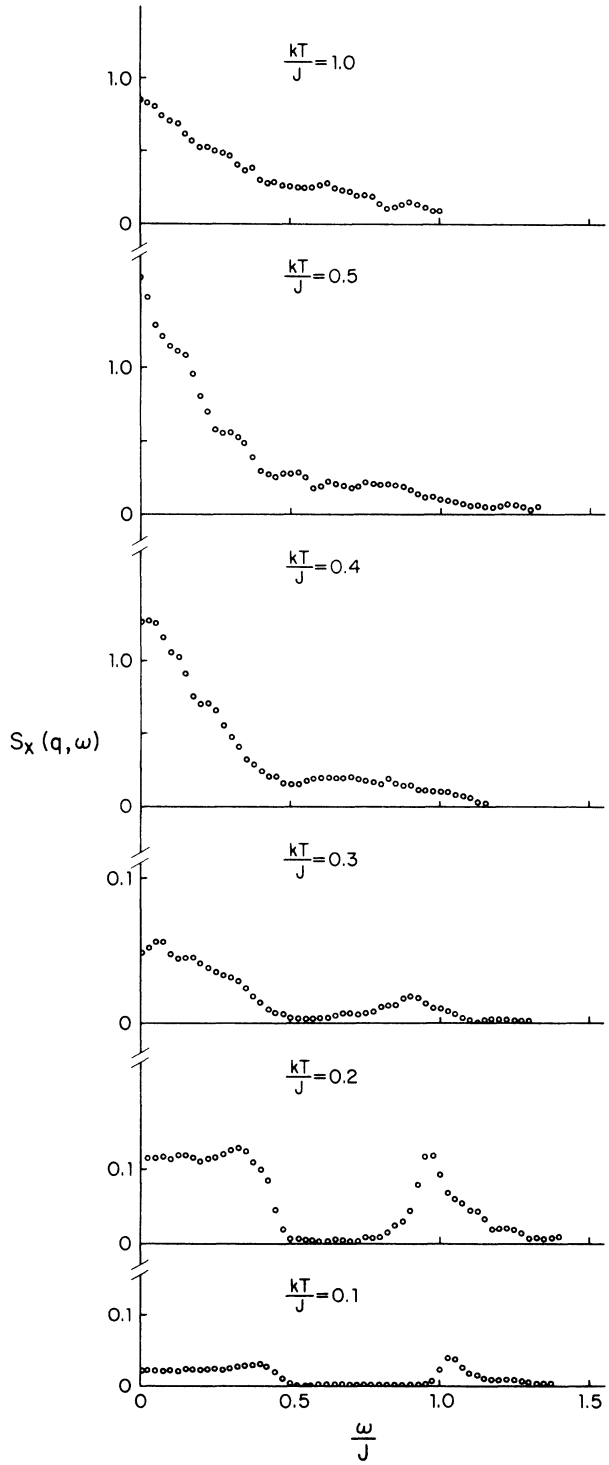

FIG. 7. $S_x(q,\omega)$ as a function of ω for different temperatures k_BT as indicated. The wave vector $qa=\pi/8$ and the magnetic field $h=0.1J$.

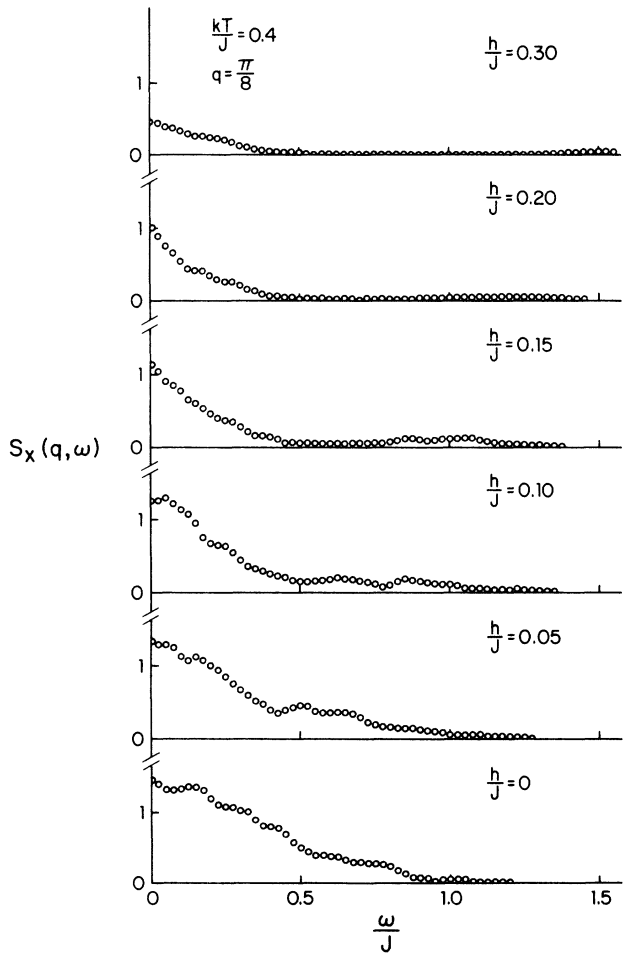

FIG. 8. $S_x(q,\omega)$ as a function of ω for different magnetic fields as indicated. The wave vector $qa=\pi/8$ and the temperature $k_BT=0.4J$.

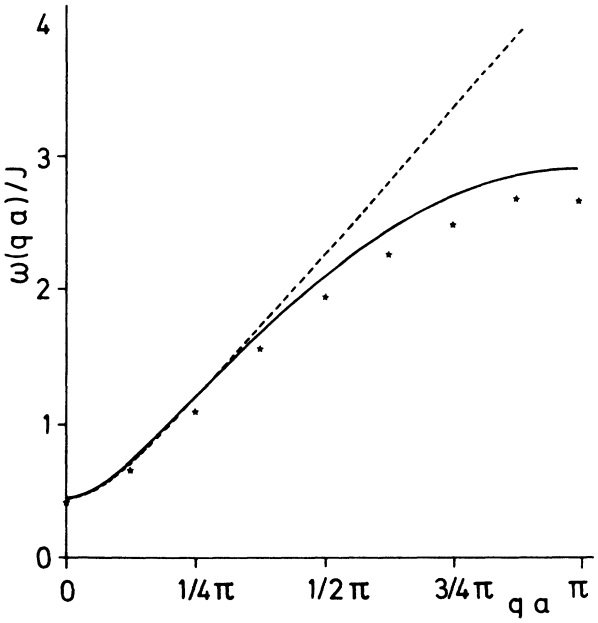

FIG. 9. The dispersion relation ω vs q for temperature $k_BT=0.2J$ and magnetic field $h=0.1J$. The data points are from the spin-dynamics simulation, the dashed line is the result for the dispersion from the sine-Gordon model, and the solid line is a harmonic approximation ($k_BT=0$) for the XY chain.

resulted from the simulation) is shown by an arrow. The position of this arrow clearly indicates that the *incorrect* position of the two theoretical curves stems from the use of the wrong dispersion relation. Nonetheless the total qualitative agreement between the theoretical prediction and the simulation results is reasonable. Due to finite temperature and a discrete lattice model (the sine-Gordon model is a continuous one) the singularity is even more smeared out.

In Fig. 11(a) we show the integrated intensity of the central soliton peak. The data are for the y polarization only because the data for the x polarization have quite large error bars; the decomposition into soliton contribution and the two-spin-wave difference process is difficult. Comparing our data with the first-order (dashed line) and second-order (solid line) approximation (17a) one clearly sees the need for higher-order theoretical corrections. Up to $k_BT=0.5J$ our points actually agree much better with the first-order than with the second-order theory.

The behavior of the HWHM given by Eq. (16) has been extracted from neutron scattering experiments by Steiner *et al.*[1,2] Depending on the main contribution to the central peak, the dominant width can either be the soliton contribution or the two-spin-wave difference process. In Fig. 7 we can clearly see a change from a dominant two-spin-wave contribution ($k_BT=0.1J$ and $k_BT=0.2J$) to a dominant soliton contribution. Figure 11(b) shows a plot of the two HWHM as a function of temperature. The y polarization shows a clear soliton contribution, whereas the x polarization shows a crossover from a two-spin-wave process (at low temperatures) to a soliton process (at higher temperatures). The value for the two-spin-

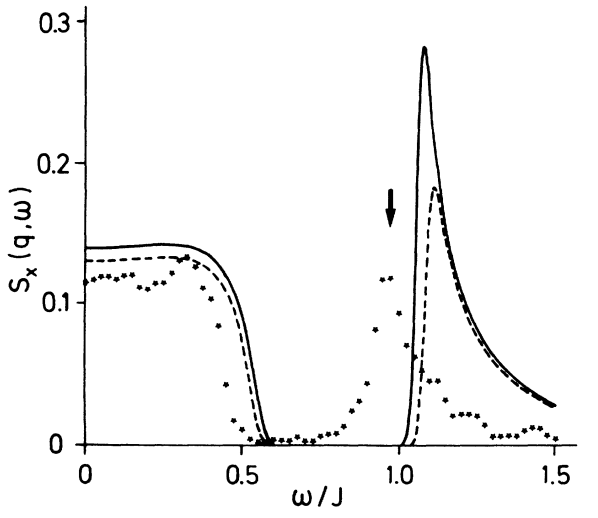

FIG. 10. $S_x(q,\omega)$ as a function of ω for temperature $k_BT=0.2J$, magnetic field $h=0.1J$, and wave vector $qa=\pi/8$. The data points ("stars") are from the simulation, the solid curve gives the prediction from the sine-Gordon model, and the dashed curve uses the dispersion relation from the harmonic approximation.

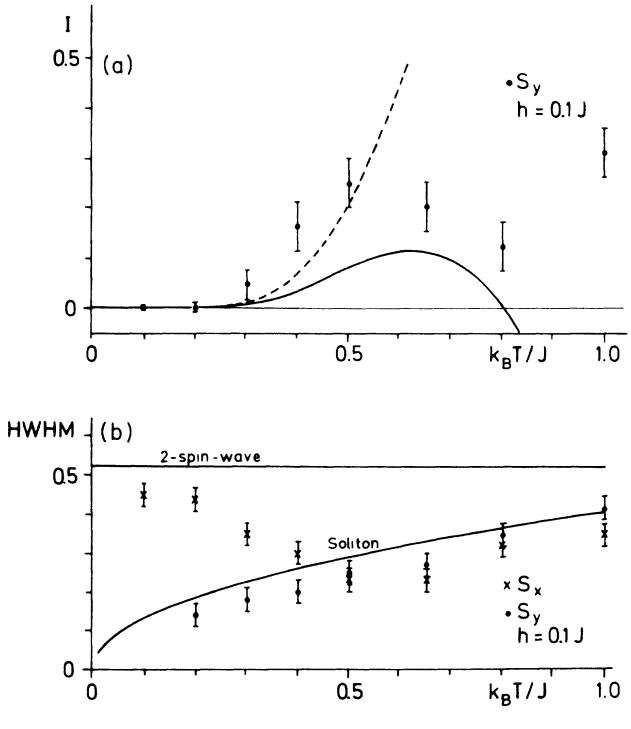

FIG. 11. (a) Integrated intensity of the central peak in $S_y(q,\omega)$ as a function of temperature. The dashed line is only the leading term from Eq. (17a) whereas the solid line is the full Eq. (17a). (b) The half-width at half maximum of the central peak for $S_x(q,\omega)$ ($\times$) and $S_y(q,\omega)$ ($\bullet$) as a function of temperature. The solid lines are the results for the two-spin-wave difference process (16b) and for the central soliton peak (16a). The magnetic field $h=0.1J$ and the wave vector $qa=\pi/8$.

wave process given in this figure is not actually determined from Eq. (16b), because cq is the cutoff value and not the HWHM. We obtained the value of the HWHM numerically, using not the value of $S_x^{\text{diff}}(q,\omega=0)$ for the maximum but the real maximum at $\omega>0$. The error bars were estimated by comparing the fitted curves with the data points. For $k_BT=0.1J$ we could not estimate a HWHM for the y polarization, because it is not possible to separate the soliton peak from the spin-wave peak, which should occur around $\omega=0.3J$ (see Fig. 4).

Comparing our Fig. 11 with Fig. (13a) of Steiner *et al.*,[2] we conclude that the experimental measurements were made at too high temperature to show the two-spin-wave process alone; the crossover from pure two-spin-wave behavior to pure soliton behavior should occur just below 4.5 K.

In Fig. 12 we show the same quantities as in Fig. 11, but as a function of magnetic field. (Note the different abscissas in Fig. 12.) In the upper part only one theoretical curve is given, because the ratio f_x/f_y is close to unity for $h<0.15J$. Within the error bars the data follow the prediction. The HWHM shows clear soliton behavior although the data points are systematically too low. From comparison with Fig. 11(b) we see that at $k_BT=0.4J$, the soliton part already dominates the two-spin-wave part.

Figure 13 shows the same properties for the y polarization as a function of wave vector. The measured integrated intensity is clearly higher as the predicted one. A

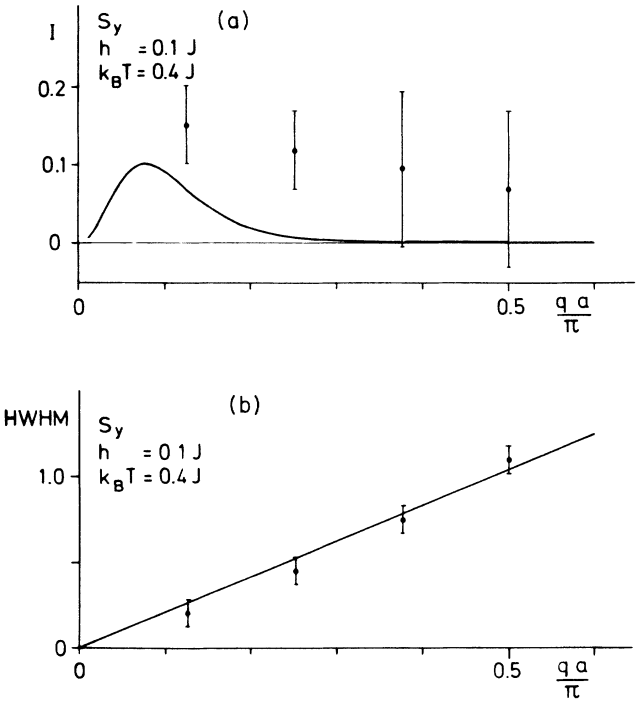

FIG. 13. (a) Integrated intensity of the central peak in $S_y(q,\omega)$ as a function of wave vector. (b) The half-width at half maximum of the central peak for $S_y(q,\omega)$ as a function of wave vector. The temperature $k_BT=0.4J$ and the magnetic field $h=0.1J$. Other parameters as in Fig. 11.

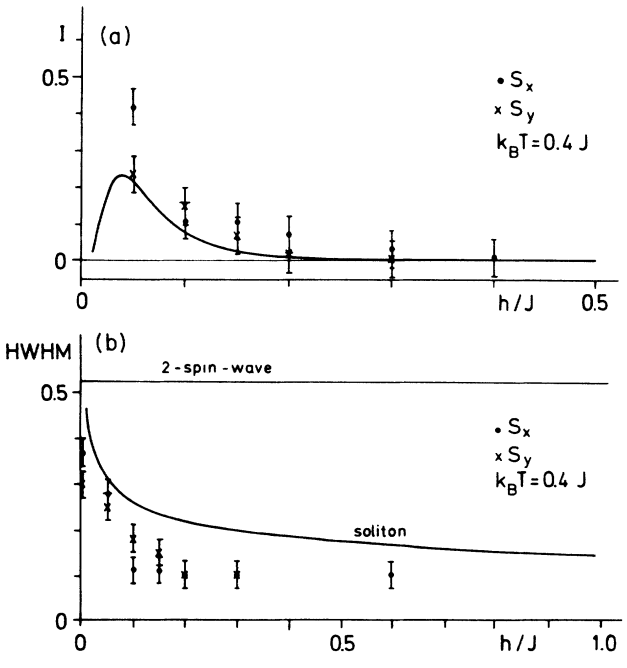

FIG. 12. (a) Integrated intensity of the central peak in $S_x(q,\omega)$ (●) and $S_y(q,\omega)$ (×) as a function of magnetic field. (b) The half-width at half maximum of the central peak for $S_x(q,\omega)$ (●) and $S_y(q,\omega)$ (×) as a function of magnetic field. The temperature $k_BT=0.4J$. Other parameters as in Fig. 11.

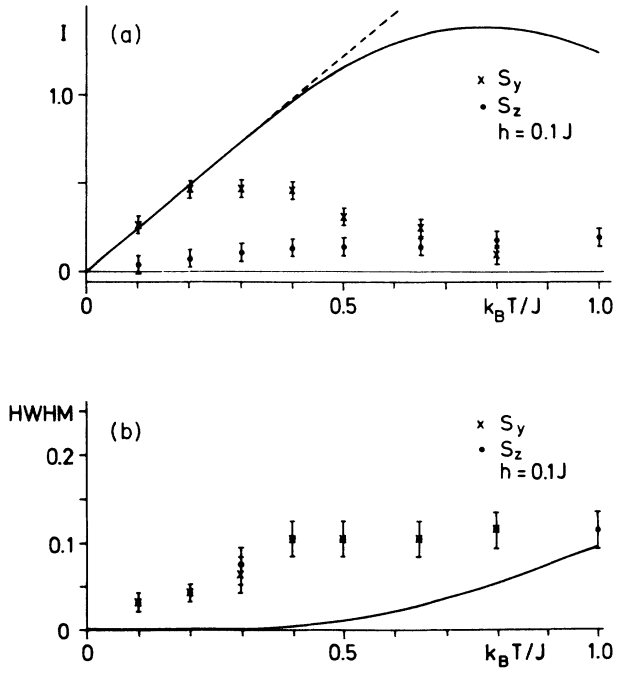

FIG. 14. (a) Integrated intensity of the spin-wave peak in $S_y(q,\omega)$ (×) and $S_z(q,\omega)$ (●) as a function of temperature. The dashed line indicates the leading term in Eq. (17c) and the solid line is the full Eq. (17c). (b) The half-width at half maximum of the spin-wave peak for $S_y(q,\omega)$ (×) and $S_z(q,\omega)$ (●) as a function of temperature. The magnetic field $h=0.1J$ and the wave vector $qa=\pi/8$.

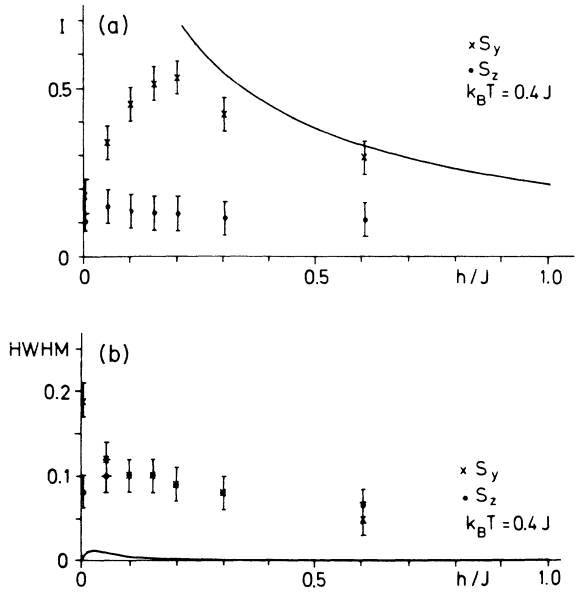

FIG. 15. (a) Integrated intensity of the spin-wave peak in $S_y(q,\omega)$ ($\times$) and $S_z(q,\omega)$ (●) as a function of magnetic field. (b) The half-width at half maximum of the spin-wave peak for $S_y(q,\omega)$ ($\times$) and $S_z(q,\omega)$ (●) as a function of magnetic field. The temperature $k_BT=0.4J$. Other parameters as in Fig. 14.

statement about the functional dependence with wave vector cannot be made. The HWHM clearly follows the predicted linear behavior. It is much easier to measure the HWHM with some given accuracy then the integrated intensity.

The integrated intensity and the HWHM of the single-spin-wave contribution are shown in Fig. 14 as a function of temperature and in Fig. 15 as a function of magnetic field. The first surprising fact is a qualitative difference between the integrated intensity, where the y and z polarizations differ substantially, and the HWHM, where both polarizations are on top of each other. The interaction of the spin waves with the solitons seems to increase the intensity but does not change the line shape of the single-spin-wave contribution. Therefore, we see no effect in the HWHM but a dramatically increased integrated intensity in the y polarization. (This interaction cannot be seen in the z polarization.) This interpretation is supported by the fact that the effect is maximal for the field-temperature range where we have the maximum soliton contribution.

The integrated intensity of the y polarization follows the theoretical prediction for $k_BT \leq 0.2J$. For higher temperatures it shows qualitatively similar behavior as the second-order approximation (solid line), but the quantitative differences might come from missing higher-order corrections. The field dependence of the integrated intensity of the y polarization for zero field is identical to that of the z polarization. Then it increases until it almost "reaches" the theoretical prediction at $h \approx 0.25J$. For larger h it lies systematically below the theoretical prediction.

The HWHM does not agree with the theoretical prediction; neither the functional dependence from temperature or field nor the quantitative values agree. The treatment of spin waves in the sine-Gordon picture is simply inadequate. The peaks have a much larger width than predicted. The difference in the HWHM for the two polarizations for small h for Fig. 15(b) has its origin in an overlap between the central soliton peak and the spin-wave peak. For $h \to 0$ the peak position also goes towards zero.

V. CONCLUSIONS

Using an ultrafast vectorized program on a CDC Cyber 205, we have calculated $S(q,\omega)$ for XY chains in an external magnetic field along the x axis. We believe that we have demonstrated that the spin-dynamics method has been developed to the point that it is a precise tool to study excitations in spin systems. This approach can also be used to study spin systems at high temperatures[26] and is clearly better than other similar methods.[27]

We compared our results with theoretical predictions in order to test the theory and we found excellent qualitative agreement with the predicted single-spin-wave, two-spin-wave, and soliton contributions to $S(q,\omega)$. The observed quantitative differences between the results from the simulation and the theoretical predictions show clearly that quantum corrections alone cannot account for the differences between theory and experiments.

The sine-Gordon mapping[8,9] is an excellent tool to classify the different contributions of the different excitations in $S(q,\omega)$. Without it, the interpretation of the results (from experiments and from simulations) would have been much more difficult. Nevertheless the quantitative agreement is not satisfactory, and further theoretical development is needed.

Our results also suggest that experimentally a clear separation of two-spin-wave and soliton contributions to the central peak can only be made with the benefit of lower temperature data. The eventual three-dimensional ordering places restrictions on the minimum useful temperature, and thus other systems with weaker interchain coupling will be needed for further experimental progress.

ACKNOWLEDGMENTS

The work was supported in part by the National Science Foundation (NSF) Grant No. DMR-8715740. One of us (R.W.G.) wishes to thank the Alexander von Humboldt Stiftung for support.

[1]M. Steiner, J. Villain, and C. G. Windsor, Adv. Phys. **25**, 87 (1976).

[2]M. Steiner, K. Kakurai, and J. K. Kjems, Z. Phys. B **53**, 117 (1983).

[3]A. P. Ramirez and W. P. Wolf, Phys. Rev. Lett. **49**, 227 (1982).

[4]J. P. Boucher, L. P. Regnault, J. Rossat-Mignot, J. P. Renard, J. Bouillot, and W. G. Stirling, J. Appl. Phys. **52**, 1956 (1982); J. P. Boucher, L. P. Regnault, A. Pires, J. Rossat-Mignot, Y. Henry, J. Bouillot, W. G. Stirling, and J. P. Renard, in *Magnetic Excitations and Fluctuations,* edited by S. W. Lovesey, U. Balucani, F. Borsa, and V. Tognetti (Springer, Berlin, 1984).

[5]F. Borsa, Phys. Rev. B **25**, 3430 (1982); F. Borsa, M. G. Pini, A. Rettori, and V. Tognetti, *ibid.* **28**, 5173 (1983).

[6]K. Kopinga, A. M. C. Tinus, and W. J. M. de Jonge, Phys. Rev. B **29**, 2868 (1984); A. M. C. Tinus, W. J. M. de Jonge, and K. Kopinga, *ibid.* **32**, 3154 (1985).

[7]T. Goto and Y. Yamaguchi, J. Phys. Soc. Jpn. **50**, 2133 (1981).

[8]H. J. Mikeska, J. Phys. C **11**, L29 (1978).

[9]E. Allroth and H. J. Mikeska, Z. Phys. B **43**, 209 (1981).

[10]C. Etrich, H. J. Mikeska, E. Magyari, H. Thomas, and R. Weber, Z. Phys. B **62**, 97 (1985).

[11]See, e.g., *Magnetic Excitations and Fluctuations,* edited by S. W. Lovesey, U. Balucani, F. Borsa, and V. Tognetti (Springer, Berlin, 1984).

[12]R. W. Gerling and D. P. Landau, J. Magn. Magn. Mater. **45**, 267 (1984).

[13]R. W. Gerling and D. P. Landau, in *Magnetic Excitations and Fluctuations,* edited by S. W. Lovesey, U. Balucani, F. Borsa, and V. Tognetti (Springer, Berlin, 1984).

[14]M. Staudinger, R. W. Gerling, C. S. S. Murty, and D. P. Landau, J. Appl. Phys. **57**, 3335 (1985).

[15]R. W. Gerling, M. Staudinger, and D. P. Landau, J. Magn. Magn. Mater. **54-57**, 819 (1986).

[16]D. P. Landau, R. W. Gerling, and M. S. S. Challa, in *Magnetic Excitations and Fluctuations II,* edited by U. Balucani, S. W. Lovesey, M. G. Rasetti, and V. Tognetti (Springer, Berlin, 1987).

[17]R. W. Gerling and D. P. Landau, Phys. Rev. B **37**, 6092 (1988).

[18]R. W. Gerling, Comp. Phys. Rep. **7**, 73 (1988).

[19]K. Binder and D. P. Landau, Phys. Rev. B **13**, 1140 (1976).

[20]See, e.g., R. L. Burden, J. D. Fairas, and A. C. Reynolds, *Numerical Analysis* (Prindle, Weber, and Schmidt, Boston, 1978).

[21]R. J. Birgeneau, J. Skalyo, and G. Shirane, Phys. Rev. B **3**, 1736 (1971); I. U. Heilmann, G. Shirane, Y. Endoh, R. J. Birgeneau, and S. L. Holt, *ibid.* **18**, 3530 (1978).

[22]J. F. Currie, J. A. Krumhansl, A. R. Bishop, and S. E. Trullinger, Phys. Rev. B **22**, 477 (1980).

[23]T. Schneider and E. Stoll, Phys. Rev. B **2**, 5317 (1980).

[24]J. A. Krumhansl and J. R. Schrieffer, Phys. Rev. B **11**, 3635 (1975).

[25]G. Reiter, Phys. Rev. Lett. **60**, 2214 (1988).

[26]R. W. Gerling and D. P. Landau, Phys. Rev. Lett. **63**, 812 (1989).

[27]G. Müller, Phys. Rev. Lett. **60**, 2785 (1988); **63**, 813 (1989).